Organic Electronics 13 (2012) 1129–1135

Contents lists available at SciVerse ScienceDirect

Organic Electronics

journal homepage: www.elsevier.com/locate/orgel

Modification of emission wavelength in organic random lasers based on photonic glass

Yujie Chen [a,*], Johannes Herrnsdorf [a], Benoit Guilhabert [a], Yanfeng Zhang [a], Alexander L. Kanibolotsky [b], Peter J. Skabara [b], Erdan Gu [a], Nicolas Laurand [a], Martin D. Dawson [a]

[a] Institute of Photonics, SUPA, University of Strathclyde, Glasgow G4 0NW, UK
[b] WestCHEM, Department of Pure and Applied Chemistry, University of Strathclyde, Glasgow G1 1XL, UK

ARTICLE INFO

Article history:
Received 6 December 2011
Received in revised form 7 February 2012
Accepted 17 March 2012
Available online 3 April 2012

Keywords:
Random laser
π-Conjugated polymer
Photonic glass
Transport mean free path

ABSTRACT

Control of the emission wavelength of a random laser (RL) system over a 7-nm waveband is demonstrated using a green-emitting π-conjugated polymer infiltrated into a photonic glass formed by nano/micro-size monodisperse silica spheres. The use of a solution-based conjugated polymer enables the complete filling of the voids within the photonic glass without suffering from quenching and the gain can therefore be maximized. The emission wavelength of these structures is set by a combination of the material system spectral gain and of the transport mean free path, the latter being controlled by the mean diameter of the spheres in the nano-scale range. Transport mean free paths of photons in the RL's active region are calculated using Mie scattering theory and corroborated with coherent backscattering measurements. Further wavelength modification is also possible by changing the pump spot size and the pump fluence.

1. Introduction

In recent years there has been a rapidly growing interest in random lasers (RLs). A RL is based on light amplification by stimulated emission via multiple scattering due to randomness in a high-gain disordered medium [1]. The interest in RLs stems not only from their intriguing concept and features but also from their potential for simple and versatile fabrication that may open up new applications. The majority of RL studies to date have focused on proof-of-concept demonstrations and basic physics without too much concern for controllability of the laser characteristics [2–8]. However, in order to develop applications, it is crucial to have at least some control over these characteristics and in particular over the emission wavelength [1]. Among other proposals and demonstrations for RL mode control [9–21], photonic glass systems formed by randomly deposited wavelength-size, monodisperse spheres are promising because they enable the modification of light diffusion properties [22,23]. For example, such assemblies of dielectric spheres exhibit sharp Mie resonances in the strong scattering regime and thus can be applied to the realization of resonance-driven RLs where the emission wavelength is controlled by the size of the spheres [24].

A photonic glass can be created via a modified self-assembly method [22]. The standard self-assembly technique is widely used to grow ordered structures such as opal-based photonic crystals [for example, see the diagram in the *left panel* of Fig. 1(a)] from colloidal suspensions of dielectric spheres [25]. The modified technique [22] enables the fabrication of new disordered materials formed by the random packing of nano/micro-size spheres [see the diagram in the *right panel* of Fig. 1(a)]. This approach is based on the modification of the charge of the colloidal spheres by the addition of salt or acid into the solution, which then provokes flocculation of the suspended particles. It is noted that a resonance-driven RL action has been

* Corresponding author.
E-mail address: yujie.chen@strath.ac.uk (Y. Chen).

1566-1199/$ - see front matter © 2012 Elsevier B.V. All rights reserved.
http://dx.doi.org/10.1016/j.orgel.2012.03.014

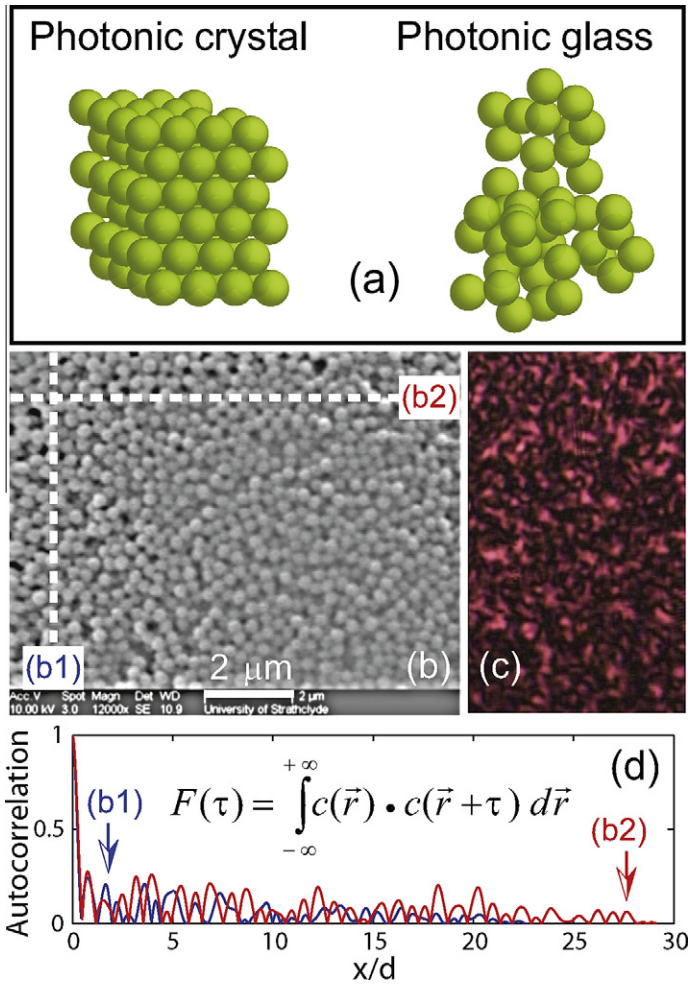

Fig. 1. (a) Nano/micro-spheres forming a photonic crystal (left panel) or photonic glass (right panel). (b) Scanning electron microscope (SEM) image of SiO_2 spheres with mean diameter of 320 nm forming a photonic glass. (c) Light speckle pattern recorded from a back scattering direction of the as-prepared photonic glass sample. (d) Autocorrelation calculation corresponding to two lines marked in the SEM image in (b).

demonstrated by using such an approach, with a photonic glass formed by polystyrene nano/micro-spheres and infiltrated with dye molecules [24].

In this work, we demonstrate RL action in an entirely solution-processable silica photonic glass gain medium incorporating a π-conjugated polymer. Conjugated semiconducting polymers have been identified as an attractive class of materials for laser applications owing to their high-emission efficiency, large cross-section for stimulated emission and wide spectral coverage [26]. As opposed to dyes, they do not quench when in a close-packed solid-state format, which means that their density and hence the optical gain can be maximized. It is then expected that the threshold fluence of conjugated polymer-based RLs will be improved (for similar structures) compared to that of dye molecule-based RLs. For example, the RL threshold of $\sim$3 mJ/cm^2 found in our study (see below) compares favorably to the DCM dye-based RL threshold of 5 mJ reported in Ref. [24]. In fact, given that the pump spot size used in Ref. [24] was stated to be 1 mm^2 in diameter, this threshold corresponds to $\sim 6.4 \times 10^2$ mJ/cm^2: the threshold of the conjugated polymer RL reported in this study is therefore two orders of magnitude lower in terms of fluence. The organic semiconductor material used is the green-emitting π-conjugated polymer poly[2,5-bis(2′,5′-bis(2″-ethylhexyloxy)phenyl)-*p*-phenylene vinylene] (BBEHP-PPV), whose chemical structure is given in Fig. 2(a). This organic semiconductor has been reported as a very promising laser material [27,28]. Particularly, it is noteworthy to point out that the molecular structure of BBEHP-PPV effectively encapsulates the polymer backbone via the attached parallel-oriented hydrocarbon side chains. This generates a protective sheath hence limiting self-quenching and potentially enhancing the resistance to photo-bleaching [27]. The photostability of BBEHP-PPV has been tested in a thin film structure on a planar glass substrate, indicating a 1/e degradation dosage of $\sim$20 J/cm^2 when pumped at a 5-ns/10-Hz laser pulse with wavelength of 355 nm under the fluence of 260 μJ/cm^2 (above gain threshold due to low loss in that case). It is thus not surprising to see no significant degradation of the polymer during our photo-pumping experiment to observe RL action at the threshold

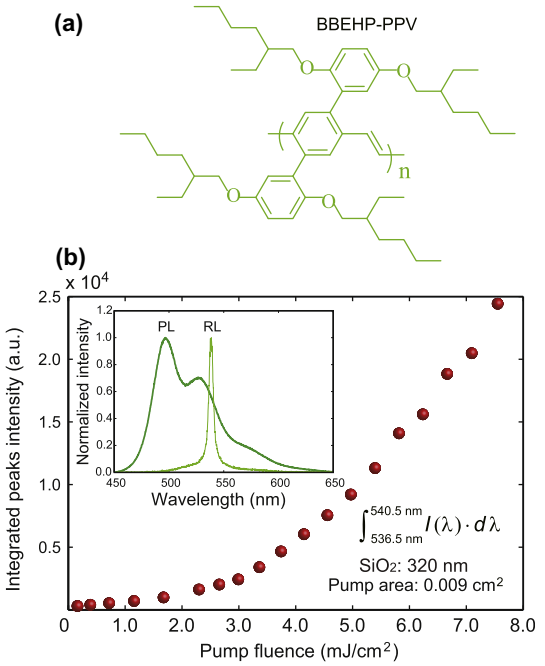

Fig. 2. (a) The chemical structure (Ref. [27]) of the gain material (BBEHP-PPV) used in the random laser experiment. (b) Integrated peak (536.5–540.5 nm) intensity as a function of the pump fluence, demonstrating a threshold characteristic behavior. (Inset) Normalized photoluminescence (PL) spectrum from a BBEHP-PPV neat film and random laser (RL) spectrum from BBEHP-PPV infiltrated into a photonic glass (sphere diameter: d = 320 nm).

in the range of several mJ/cm^2 (with estimated total exposure time under laser pumping for each sample of no more than 5 min). The photonic glass used here is made of silica spheres rather than polymer spheres and is consequently more robust and resistant to solvent exposure. This is a critical feature for full solution-processability of the RL structure because toluene was used to dissolve the gain polymer (BBEHP-PPV) thus making it solution processable. Experimentally, it is found that the RL emission spectral peak under photo-pumping can be shifted over 3-nm by varying the transport mean free paths in the photonic glass random systems. The individual Mie resonances are washed-out due to the combined effect of modest refractive index contrast between the silica spheres and BBEHP-PPV and the size dispersity of the spheres. Further emission wavelength modification (over ~7 nm) is possible via changing the pump spot area, as well as the pump fluence.

2. Experimental section

We prepared a series of photonic glass samples formed by nano/micro-size silica spheres with mean diameters (d) ranging from 150 nm to 3000 nm (Bangs Laboratories Inc.). These silica spheres are supplied in suspension in an aqueous solution at a concentration of 100 mg/ml. The size dispersity is below 10% for each specified diameter. A 10% volume of 0.5 M HCl was added to the solution to provoke the flocculation of the suspended nano/micro-spheres. About 100 μl of the charged solution was then drop-coated onto a clean glass substrate to form a photonic glass sample with specific sphere size. The as-prepared samples were then left in a dry place for two days to allow the water to fully evaporate. The thickness (L) of the respective photonic glasses was in the range of 200–600 μm as measured under a microscope and the filling fraction (η) is about 50–60% according to a study presented in the literature [23]. The scanning electron microscope (SEM) image of a 320-nm-diameter SiO_2 sphere assembly is shown in Fig. 1(b). The randomness of the as-prepared photonic glass sample was confirmed [22] via measuring the light speckle pattern [Fig. 1(c)] and via autocorrelation inspection of the SEM image [Fig. 1(d)]. Powder BBEHP-PPV (the synthesis method can be found elsewhere [27]) was dissolved into toluene solution at a concentration of 20 mg/ml, followed by an ultrasonic bath for at least 1 min to allow the polymer to be dissolved completely. BBEHP-PPV/toluene solution was then drop-coated onto the photonic glass samples several times, allowing the gain material to infiltrate into the voids.

The active photonic glass samples were photo-pumped at a 45-degree angle to the surface normal by a frequency-tripled Q-switched Nd:YAG laser system, yielding 5-ns pump pulses at a repetition rate of 10 Hz with an excitation wavelength of 355 nm. The pump spot size could be set in the range of 0.0024–0.353 cm^2 by placing an optional spherical lens in the pump light path and was monitored by a CCD camera. Emission normal to the sample was collected by a 50-μm-core optical fiber connected to a multi-channel grating-CCD spectrometer (Avantes: spectral resolution of 0.13 nm).

3. Results and discussion

Fig. 2(b) shows the RL characteristics obtained by photo-pumping a system made with 320-nm spheres. The main plot is the integrated intensity – from 536.5 to 540.5 nm – as a function of the pump fluence and presents a threshold, a signature of laser action [1,26], at ~3 mJ/cm^2 (pump spot area: 0.009 cm^2). The relative 'softness' in the threshold turn-on can be explained by spontaneous emission coupled into the large number of laser modes [8,29]. The inset of Fig. 2(b) shows the normalized photoluminescence (PL) spectrum from a neat film of BBEHP-PPV and a typical RL spectrum from BBEHP-PPV infiltrated into the photonic glass random system (d = 320 nm). The emission spectrum becomes much narrower when pumping above the threshold, which is another signature of laser action [1,26]. The full width at half maximum (FWHM) of the RL spectrum shown here is slightly broad (~3.5 nm) though multiple peaks can be observed on top of the spectrum, due to the fact that in a diffusive RL system, many overlapping lasing modes exist and compete [30,31]. It is also found that for a small active region volume (small pump spot area), the RL spectrum slightly narrows and becomes 'spiky' (i.e. separated narrow peaks appear on top of the broader stimulated emission spectrum) as demonstrated below. In the rest of the Letter, for the investigation of the modification of the RL's spectrum, we refer to the central wavelength of the emission spectrum as the peak and study the shift of its position for different parameters.

Random laser systems formed by monodisperse nano/micro-spheres with different diameters were investigated. The influence of the size of the spheres on the laser emission wavelength for various pump fluences and with large (0.353 cm^2) or small (0.005 cm^2) pump spot areas are summarized in Fig. 3. It can be seen that with the same pump spot area and pump fluence, the RL emission peak wavelength blueshifts as the size of the silica spheres increases. This behavior is mainly attributed to the difference in transport mean free paths between the photonic glass systems having different sphere sizes. The transport mean free path is a key factor linked to multiple scattering [24,32,33] and is determined as the average distance above which the scattering wave is randomized [34], which will be elaborated in the following.

In order to gain more understanding on how the nano/micro-spheres have an impact on the peak emission wavelength, we applied the Mie scattering theory to map out the wavelength-dependent transport mean free path of our system. In the weak-scattering regime (which is valid in our case because the modest index contrast between scatterers and the gain medium leads to a transport mean free path of light much larger than the wavelength; see below), the wavelength-dependent transport mean free path $\ell_t(\lambda)$ (which should be far less than the sample thickness L for multiple scattering) can be estimated through the following formula [32,33]:

$$\ell_t(\lambda) = \frac{1}{\rho\sigma_t(\lambda)} \tag{1}$$

where $\rho = \eta/(4\pi a^3/3)$ is the density of spheres with filling fraction η ($\eta = 50\%$ was used to do the calculation in the following), and $\sigma_t(\lambda)$ is wavelength-dependent transport scattering cross-section. The definitions of scattering cross-section (σ_{sc}) and its corresponding asymmetry cross-section (σ_{asym}) are given by [35]:

$$\sigma_{sc} = \int d\Omega |f(\theta)|^2 \tag{2}$$

$$\sigma_{asym} = \int d\Omega |f(\theta)|^2 cos\theta \tag{3}$$

where $|f(\theta)|$ is the scattering amplitude. The transport scattering cross-section can then be expressed as [36]:

$$\sigma_t = \int d\Omega |f(\theta)|^2 (1 - cos\theta) = \sigma_{sc} - \sigma_{asym} \tag{4}$$

In terms of scattering by a solid dielectric sphere with radius a and refractive index n_{sph}, the scattering cross-section is given by [32,35]:

$$\sigma_{sc} = (2\pi/k^2)\sum_{n=1}^{\infty}(2n+1)(|a_n|^2 + |b_n|^2) \tag{5}$$

where $k = 2\pi n_{sur}/\lambda_0$ is the wave vector in the surrounding medium with refractive index n_{sur} and λ_0 is the free space scattering wavelength. Here, a_n and b_n are the scattering coefficients that are given by:

$$a_n = \frac{m\psi_n(mx)\psi_n'(x) - \psi_n(x)\psi_n'(mx)}{m\psi_n(mx)\xi_n'(x) - \xi_n(x)\psi_n'(mx)} \tag{6}$$

and

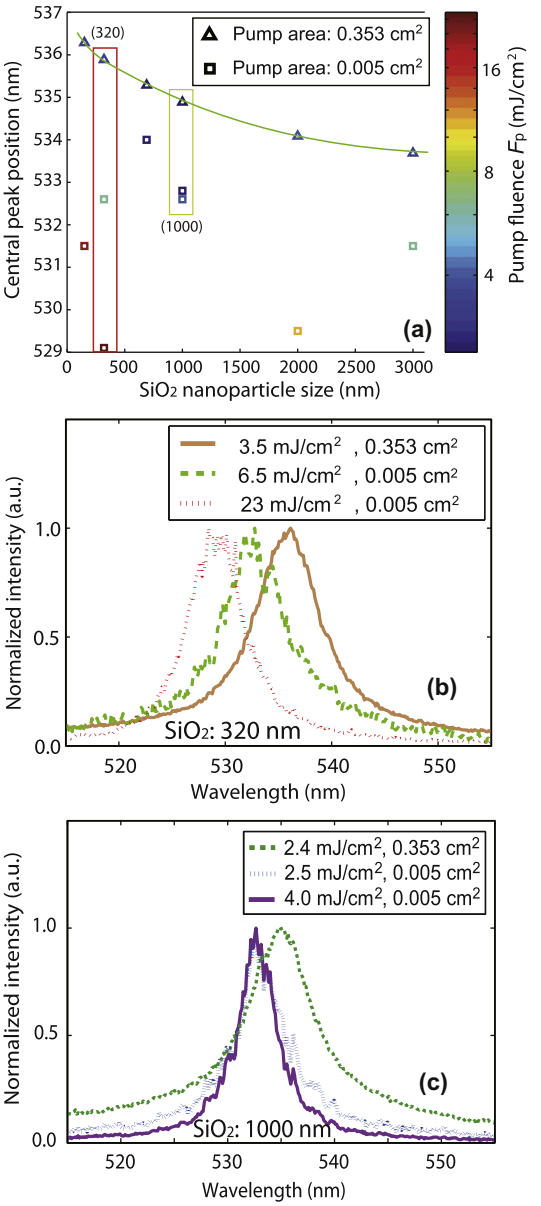

Fig. 3. (a) Relationship between random laser emission central peak, pump fluence (F_p) and SiO_2 sphere size with typical spectra from the photonic system formed by (b) 320-nm and (c) 1000-nm diameter SiO_2 spheres.

$$b_n = \frac{\psi_n(mx)\psi_n'(x) - m\psi_n(x)\psi_n'(mx)}{\psi_n(mx)\xi_n'(x) - m\xi_n(x)\psi_n'(mx)} \tag{7}$$

The parameters of m and x are obtained by the relations $m = n_{sph}/n_{sur}$ and $x = ka$, respectively, while $\lambda_0\psi_n(r) = rj_n(r)$ and $\xi_n(r) = rh_n^{(1)}(r)$, with $j_n(r)$ and $h_n^{(1)}(r)$ the Bessel and Hankel spherical functions of the first type. The asymmetry cross-section is then [35]:

$$\sigma_{asym} = (2\pi/k^2)\sum_{n=1}^{\infty}\left[\frac{2n+1}{n+1}Re(a_n b_n^*) + \frac{n(n+2)}{n+1}Re(a_n a_{n+1}^* + b_n b_{n+1}^*)\right] \tag{8}$$

In our case, we have $n_{sph} = 1.46$ for silica spheres and $n_{sur} = 1.7$ ($\Delta n = |n_{sph} - n_{sur}| = 0.24$) for BBEHP-PPV (Ref. [27]) and the corresponding wavelength-dependent transport mean free paths were calculated for various sphere sizes. As a comparison, the transport mean free path for the case where no gain material is infiltrated into the photonic glass ($\Delta n = 0.46$) was also calculated. The results are shown in Fig. 4. The transport mean free paths increase ~5-fold and the Mie resonances are smoothed out going from an index contrast $\Delta n = 0.46$ [Fig. 4(a)] to $\Delta n = 0.24$ [Fig. 4(b)]. While, as shown in Fig. 4(b), the Mie resonances are still present within the spectral window of the organic semiconductor emission (except for the smallest sphere size $d = 150$ nm), their reduced strength means that their overall contribution to the transport mean free paths is negligible (<5%), especially if we take the sphere size dispersity (<10% in our case) into account. Thus Mie resonances are expected to have a negligible, or at the very least weak, effect in setting the RL wavelength in the present RL system.

In Fig. 4(b), it is seen that ℓ_t increases with the diameter of the spheres. This can be confirmed via coherent backscattering (CBS) measurement [37,38], and the experimental values of ℓ_t can be obtained by fitting the CBS cone [Fig. 5] using the simplified diffusion CBS model [39,40]. Table 1 presents a comparison of the transport mean free path between the calculated and experimental values. The results are consistent, although there is a small discrepancy for bigger spheres. This is mainly due to the simplified assumption for the calculation of ℓ_t simply based on the density of spheres with an estimated filling fraction [32], which will have increasing discrepancy for bigger spheres with about 10% size dispersity. However, it is clear that the transport mean free path is at least an order of magnitude larger than the wavelength of interest. According to the Ioffe–Regel criterion ($\lambda \ll \ell_t$) [41], our photonic glass random laser system operates in the diffusive regime. It is known that in this regime, as can be found by analyzing the rate equations, the random lasing process is dominated by ℓ_t where $\ell_t \ll L$ (the sample thickness) is a prerequisite for multiple light scattering [24].

A longer transport mean free path leads to RL modes which overall interact less with the gain volume, i.e. the photon lifetime in the amplifying region is shorter. Because conjugated polymers are quasi-three level laser systems with non-zero (though small) re-absorption [26], the RL emission wavelength of devices with bigger spheres, hence

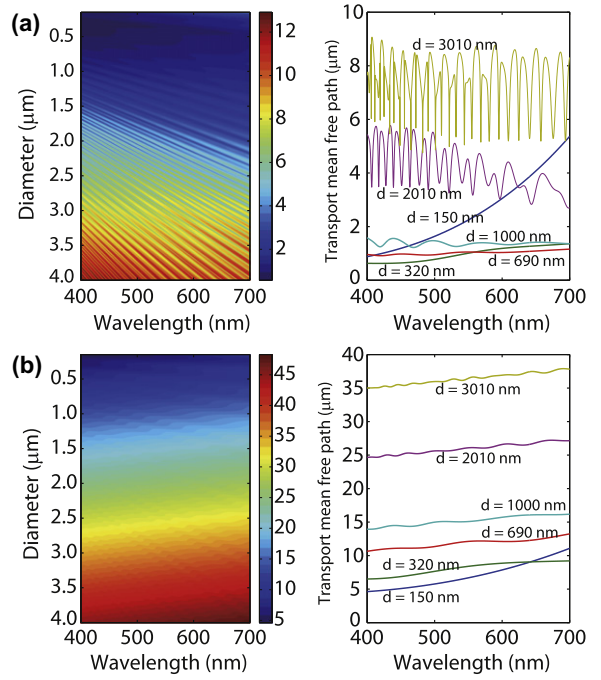

Fig. 4. (left panel) Map of calculated transport mean free path for a random system formed by monodisperse silica spheres ($n_{sph} = 1.46$) surrounded by (a) air and (b) BBEHP-PPV ($n_{sur} = 1.7$). (right panel) Plot of transport mean free path versus wavelength for those silica spheres with specific mean diameters used in the experiment.

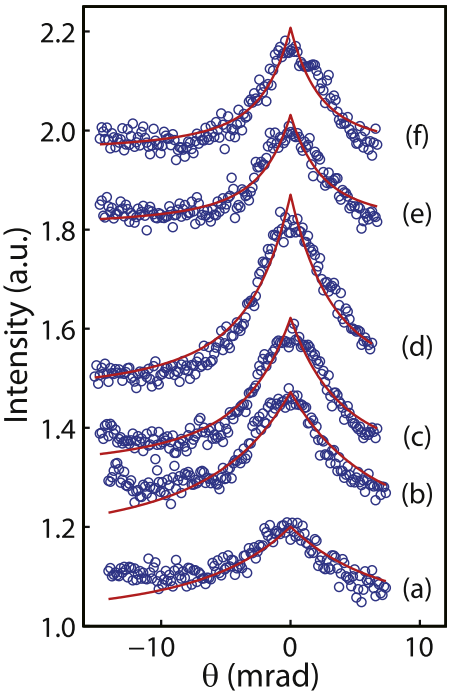

Fig. 5. Coherent backscattering (CBS) cone measured (using a He–Ne laser with wavelength of 633 nm) from the as-prepared photonic glass RL samples: (a) d = 150 nm, (b) d = 320 nm, (c) d = 690 nm, (d) d = 1000 nm, (e) d = 2010 nm, and (f) d = 3010 nm. The data points are fitted to the CBS model to extract the corresponding ℓ_t.

Table 1
Transport mean free path ℓ_t ($\lambda = 633$ nm) for the as-prepared photonic glass RL samples.

d (nm)	Calculated ℓ_t (μm)	Experimental ℓ_t (μm)
150	8.8	7.8 (0.5)
320	9.0	8.6 (1.0)
690	12.2	14.0 (1.2)
1000	16.0	16.1 (0.5)
2010	26.5	21.2 (2.1)
3010	37.2	24.0 (1.9)

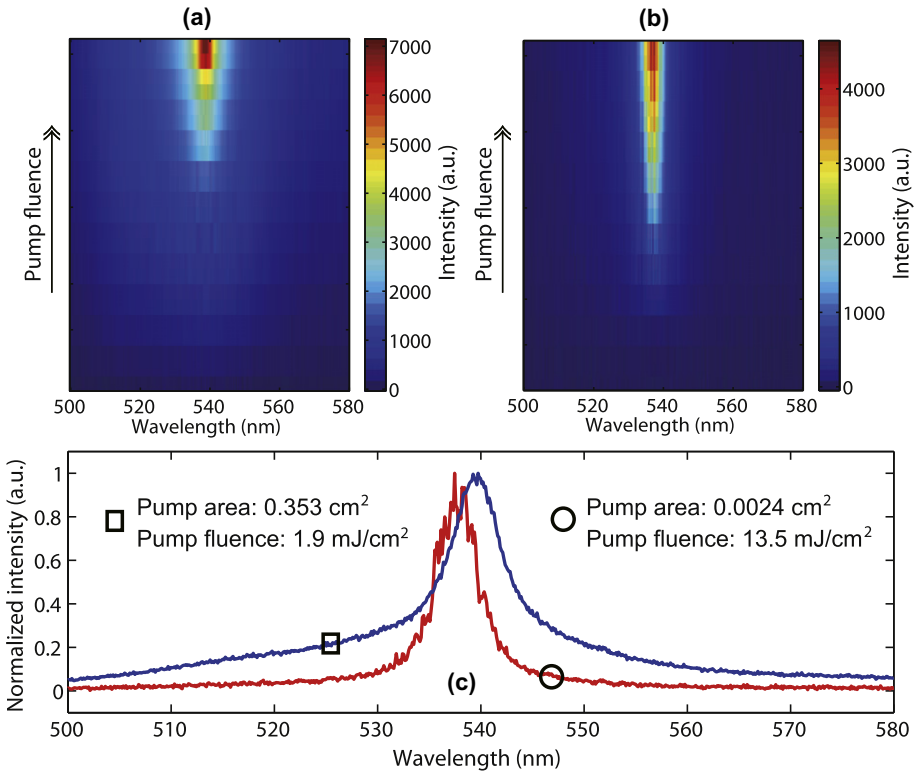

Fig. 6. Spectral evolution as a function of pump fluence: (a) pump area: 0.353 cm^2 and (b) pump area: 0.0024 cm^2. (c) Normalized emission spectra for the cases of the two different pump spot areas shown in (a) and (b), respectively. The reason for the different pump fluences shown here is that the RL signals reached their own saturation for both cases. All results are for a photonic glass containing 320-nm diameter spheres.

longer transport mean free paths, is blue-shifted as found experimentally [Fig. 3(a)]. While wider wavelength shift is obtained with resonance-driven RL, our diffusive photonic glass RL benefits from the high-gain and relative low threshold conferred by the conjugated polymer. We also note that the 3-nm waveband modification is similar to the RL stimulated emission linewidth (3.5-nm FWHM).

Two other factors – the area of the pump spot size and the strength of the pump fluence – can also have an effect on the emission wavelength and can be varied in order to further modify the RL emission wavelength [42–44]. For any of our photonic glass RLs, a smaller pump spot generates a blueshifted emission under the same pump fluence [Fig. 3(a) and (b)]. Furthermore, for the same pump spot area and same diameter of silica spheres, increasing the pump fluence blueshifts the emission central peak position as shown in the rectangular framed data points in Fig. 3(a) corresponding to the spectra shown in Fig. 3(b) and (c).

To further demonstrate the effect of the pump area on the RL wavelength, we studied a RL formed by spheres with mean diameter of 320 nm. Spectral evolution as a function of pump fluence was investigated under photo-pumping with two different pump spot areas [Fig. 6]. It is seen that the overall emission spectrum is narrower (FWHM: ~3 nm) and shows sub-structures or peaks for a small pump spot area (0.0024 cm^2) compared to the result (FWHM: ~5 nm) obtained from a big pump spot area (0.353 cm^2) [see Fig. 6(c)]. We then plotted in Fig. 7 the laser threshold and the central emission peak position as a function of the

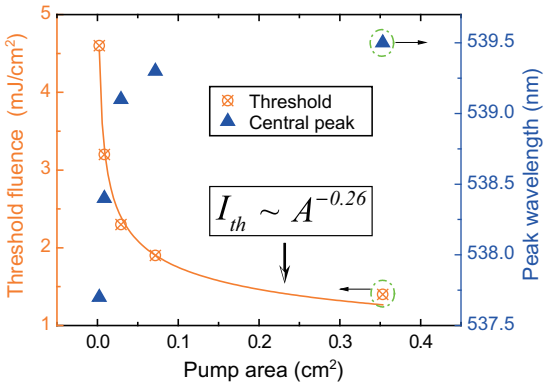

Fig. 7. Evolution of threshold (I_{th}) and central peak position versus pump spot area (A) for a photonic glass containing 320-nm diameter spheres.

pump spot area. The central peak position blueshifts for a smaller pump spot agreeing with the result of Fig. 3, while the laser threshold increases [Fig. 7]. Again, such a spectral blueshift is due to the quasi-three level nature of the organic semiconductor BBEHP-PPV: self-absorption decreases under higher photo-pumping (thus increasing the emitted photon density) or for shorter total interaction length (due to the decrease of gain volume for a smaller pump area). Depletion of the ground state might also play a role by reducing re-absorption. The reason for the change of lasing

threshold is that when increasing the pump spot area, emitted photons (in larger gain volume) have a larger chance to trigger stimulated emission events hence generating more gain to compensate for the losses [45]. It is noted that the dependence of threshold fluence (I_{th}) on the pump spot area (A) has been studied in several other cases, showing a similar trend, though its exact mathematical description is still debated [7,46–48]. In our RL system here, the experimental data of I_{th} against A can be fitted to the power law by the formula of $I_{th} \sim A^{-s}$ ($s = 0.26$).

4. Conclusions

In summary, we have reported a photonic glass random laser that uses green-emitting π-conjugated polymer, BBEHP-PPV, as a gain medium and can be modified over a 7-nm waveband. The conjugated polymer enables complete filling of the voids within the photonic glass without suffering from quenching and the gain can therefore be maximized. Silica nano/micro-spheres were chosen to form the photonic glass in order to withstand a wide range of solvents and make the RL fabrication entirely solution-processable. The resulting RLs operate in the diffusive regime. The emission wavelength is shifted by changing the size of the spheres in the nano-scale range, thereby altering the transport mean free path, and/or by varying the pump spot size and pump fluence. Therefore, such active solution-processable polymer-based photonic glass systems can be promising candidates for RL applications requiring emission wavelength modification.

Acknowledgments

This work was supported by UK EPSRC under HYPIX project. Y. Chen thanks the financial support from Scottish Universities Physics Alliance (SUPA).

References

[1] D.S. Wiersma, Nat. Phys. 4 (2008) 359–367.
[2] N.M. Lawandy, R.M. Balachandran, A.S.L. Gomes, E. Sauvain, Nature 368 (1994) 436–438.
[3] H. Cao, Y.G. Zhao, S.T. Ho, E.W. Seelig, Q.H. Wang, R.P.H. Chang, Phys. Rev. Lett. 82 (1999) 2278–2281.
[4] R.C. Polson, A. Chipouline, Z.V. Vardeny, Adv. Mater. 13 (2001) 760–764.
[5] D. Anglos, A. Stassinopoulos, R.N. Das, G. Zacharakis, M. Psyllaki, R. Jakubiak, R.A. Vaia, E.P. Giannelis, S.H. Anastasiadis, J. Opt. Soc. Am. B 21 (2004) 208–213.
[6] A. Costela, I. Garcia-Moreno, L. Cerdan, V. Martin, O. Garcia, R. Sastre, Adv. Mater. 21 (2009) 4163–4166.
[7] X. Meng, K. Fujita, S. Murai, K. Tanaka, Phys. Rev. A 79 (2009) 053817.
[8] Y. Chen, J. Herrnsdorf, B. Guilhabert, Y. Zhang, I.M. Watson, E. Gu, N. Laurand, M.D. Dawson, Opt. Express 19 (2011) 2996–3003.
[9] H. Cao, J.Y. Xu, D.Z. Zhang, S.-H. Chang, S.T. Ho, E.W. Seelig, X. Liu, R.P.H. Chang, Phys. Rev. Lett. 84 (2000) 5584–5587.
[10] D.S. Wiersma, S. Cavalieri, Nature 414 (2001) 708–709.
[11] C. Vanneste, P. Sebbah, Phys. Rev. E 71 (2005) 026612.
[12] S. Xiao, Q. Song, F. Wang, L. Liu, J. Liu, L. Xu, IEEE J. Quant. Electron. 43 (2007) 407–410.
[13] C.J.S. de Matos, L.deS. Menezes, A.M. Brito-Silva, M.A. Martinez Gámez, A.S.L. Gomes, C.B. de Araújo, Phys. Rev. Lett. 99 (2007) 153903.
[14] Q. Song, S. Xiao, X. Zhou, L. Liu, L. Xu, Y. Wu, Z. Wang, Opt. Lett. 32 (2007) 373–375.
[15] Q. Song, L. Liu, L. Xu, Y. Wu, Z. Wang, Opt. Lett. 34 (2009) 298–300.
[16] H. Ying Yang, S. Fung Yu, S. Ping Lau, J. Cryst. Growth 312 (2009) 16–18.
[17] C.-R. Lee, J.-D. Lin, B.-Y. Huang, T.-S. Mo, S.-Y. Huang, Opt. Express 18 (2010) 25896–25905.
[18] J.-K. Yang, S.V. Boriskina, H. Noh, M.J. Rooks, G.S. Solomon, L.D. Negro, H. Cao, Appl. Phys. Lett. 97 (2010) 223101.
[19] S.K. Turitsyn, S.A. Babin, A.E. El-Taher, P. Harper, D.V. Churkin, S. Kablukov, J.D. Ania-Castañón, V. Karalekas, E.V. Podivilov, Nat. Photon. 4 (2010) 231–235.
[20] C.-R. Lee, J.-D. Lin, B.-Y. Huang, S.-H. Lin, T.-S. Mo, S.-Y. Huang, C.-T. Kuo, H.-C. Yeh, Opt. Express 19 (2011) 2391–2400.
[21] M. Leonetti, C. Conti, C. Lopez, Nat. Photon. 5 (2011) 615–617.
[22] P. García, R. Sapienza, A. Blanco, C. López, Adv. Mater. 19 (2007) 2597–2602.
[23] P.D. García, R. Sapienza, C. López, Adv. Mater. 22 (2010) 12–19.
[24] S. Gottardo, R. Sapienza, P.D. García, A. Blanco, D.S. Wiersma, C. López, Nat. Photon. 2 (2008) 429–432.
[25] J.F. Galisteo-López, M. Ibisate, R. Sapienza, L.S. Froufe-Pérez, A. Blanco, C. López, Adv. Mater. 23 (2011) 30–69.
[26] I.D.W. Samuel, G.A. Turnbull, Chem. Rev. 107 (2007) 1272–1295.
[27] A. Rose, Z. Zhu, C.F. Madigan, T.M. Swager, V. Bulović, Nature 434 (2005) 876–879.
[28] Y. Chen, J. Herrnsdorf, B. Guilhabert, A.L. Kanibolotsky, A.R. Mackintosh, Y. Wang, R.A. Pethrick, E. Gu, G.A. Turnbull, P.J. Skabara, I.D. Samuel, N. Laurand, M.D. Dawson, Org. Electron. 12 (2011) 62–69.
[29] J. Herrnsdorf, B. Guilhabert, Y. Chen, A. Kanibolotsky, A. Mackintosh, R. Pethrick, P. Skabara, E. Gu, N. Laurand, M. Dawson, Opt. Express 18 (2010) 25535–25545.
[30] J. Andreasen, H. Cao, Opt. Express 19 (2011) 3418–3433.
[31] H.E. Türeci, L. Ge, S. Rotter, A.D. Stone, Science 320 (2008) 643–646.
[32] E. Akkermans, G. Montambaux, Mesoscopic Physics of Electrons and Photons, Cambridge University Press, Cambridge, UK, 2007.
[33] X.H. Wu, A. Yamilov, H. Noh, H. Cao, E.W. Seelig, R.P.H. Chang, J. Opt. Soc. Am. B 21 (2004) 159–167.
[34] D.S. Wiersma, A. Lagendijk, Phys. Rev. E 54 (1996) 4256–4265.
[35] C.F. Bohren, D.R. Huffman, Absorption and Scattering of Light by Small Particles, Wiley–VCH, New York, 1998.
[36] K. Busch, C.M. Soukoulis, E.N. Economou, Phys. Rev. B 50 (1994) 93–98.
[37] G. Labeyrie, F. de Tomasi, J.-C. Bernard, C.A. Müller, C. Miniatura, R. Kaiser, Phys. Rev. Lett. 83 (1999) 5266–5269.
[38] M. Gurioli, F. Bogani, L. Cavigli, H. Gibbs, G. Khitrova, D.S. Wiersma, Phys. Rev. Lett. 94 (2005) 183901.
[39] E. Akkermans, P.E. Wolf, R. Maynard, Phys. Rev. Lett. 56 (1986) 1471–1474.
[40] D.S. Wiersma, M.P. van Albada, B.A. van Tiggelen, A. Lagendijk, Phys. Rev. Lett. 74 (1995) 4193–4196.
[41] S. John, Phys. Rev. Lett. 53 (1984) 2169–2172.
[42] S. Yu, C. Yuen, S. Lau, W. Park, G. Yi, Appl. Phys. Lett. 84 (2004) 3241.
[43] A. Vutha, S. Tiwari, R. Thareja, J. Appl. Phys. 99 (2006) 123509.
[44] A. Stassinopoulos, R.N. Das, S.H. Anastasiadis, E.P. Giannelis, D. Anglos, J. Opt. 12 (2010) 024006.
[45] G. van Soest, M. Tomita, A. Lagendijk, Opt. Lett. 24 (1999) 306–308.
[46] Y. Ling, H. Cao, A.L. Burin, M.A. Ratner, X. Liu, R.P.H. Chang, Phys. Rev. A 64 (2001) 063808.
[47] V.M. Apalkov, M.E. Raikh, Phys. Rev. B 71 (2005) 054203.
[48] F.A. Pinheiro, L.C. Sampaio, Phys. Rev. A 73 (2006) 013826.